

NeuralNEB – Neural Networks can find Reaction Paths Fast

Mathias Schreiner¹

Arghya Bhowmik²

Tejs Vegge²

Peter Bjørn Jørgensen²

Ole Winther^{1,3,4}

¹ DTU Compute, Technical University of Denmark (DTU)

² DTU Energy, Technical University of Denmark (DTU)

³ Department of Biology, University of Copenhagen (UCph)

⁴ Genomic Medicine, Copenhagen University Hospital, Rigshospitalet

Abstract

Quantum mechanical methods like Density Functional Theory (DFT) are used with great success alongside efficient search algorithms for studying kinetics of reactive systems. However, DFT is prohibitively expensive for large scale exploration. Machine Learning (ML) models have turned out to be excellent emulators of small molecule DFT calculations and could possibly replace DFT in such tasks. For kinetics, success relies primarily on the models' capability to accurately predict the Potential Energy Surface (PES) around transition-states and Minimal Energy Paths (MEPs). Previously this has not been possible due to scarcity of relevant data in the literature. In this paper we train state of the art equivariant Graph Neural Network (GNN)-based models on around 10.000 elementary reactions from the recently published Transition1x dataset. We apply the models as potentials for the Nudged Elastic Band (NEB) algorithm and achieve a Mean Average Error (MAE) of 0.13 ± 0.03 eV on barrier energies on unseen reactions. We compare the results against equivalent models trained on QM9x and ANI1x. We also compare with and outperform Density Functional based Tight Binding (DFTB) on both accuracy and required computational resources. The implication is that ML models are now at a level where they, given relevant data, aptly can be applied for studying reaction kinetics.

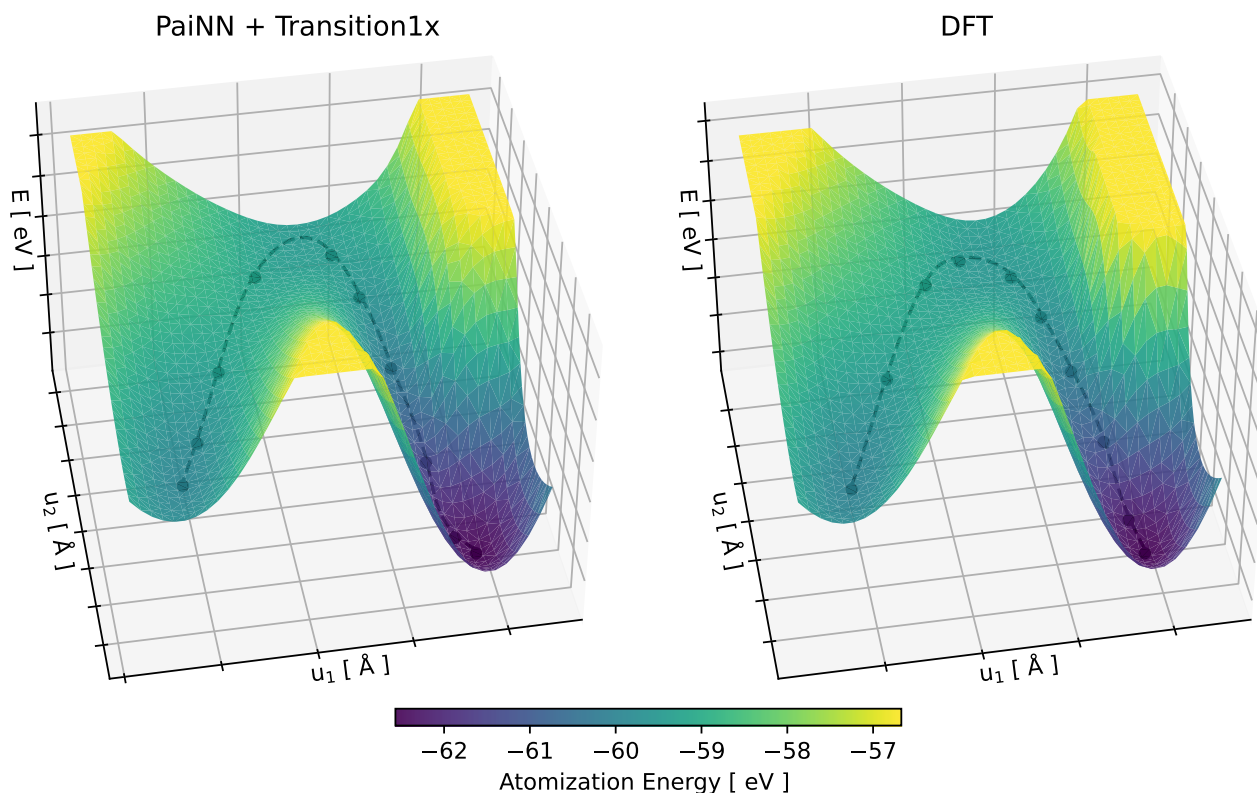


Figure 1: Minimal Energy Paths (MEPs) found with Nudged Elastic Band (NEB) applying the Graph Neural Network (GNN) architecture PaiNN trained on the Transition1x dataset and Density Functional Theory (DFT) as potentials. The MEPs are projected onto the planes in structural space, intersecting product, reactant and transition-state of the converged MEPs. The PES has been calculated on the planes in the vicinity of the MEPs with the respective potential and is shown with colors and on the z-axis. The x and y-axes are basis vectors describing the plane. The reaction involves a H-transfer coupled with a C-C bond formation on C6H8. The reaction can be seen as a GIF by following [this link](#).

1 Introduction

ML models and especially GNNs^{1,2} have turned out to be potent emulators of DFT potentials for small molecules^{3,4,5,6,7}, thanks to their remarkable ability to find complex relations in high dimensional data. They have a complexity-scaling orders of magnitudes lower than classic Quantum Mechanics (QM) methods, but have in recent years achieved comparable accuracy^{8,9,10,11,12}. The capability of these models is manifested by their success in tasks beyond simple prediction of molecular features such as structural optimization or studying finite-temperature dynamical properties through molecular dynamics^{13,14}. Despite their achievements, there has only been limited success in applying ML-models as potentials for transition search algorithms. The earliest work studied simple diatomic molecule dissociation and achieved acceptable accuracy with tens of thousands of data points¹⁵. Other works have had success by limiting their scope to studying single or few reactions but sacrificing the generality of the approach^{16,17,18}. Attempts to study reactive systems with Gaussian Processes (GPs)¹⁹ have been successful too, but the GP is trained on the particular atomic system, sacrificing speed for generality by requiring expensive DFT calculations at inference time. Transition-states are notoriously hard to find as there is no well-defined gradient on the PES to guide traditional optimization algorithms towards them. A wealth of algorithms have been proposed to solve this problem – one is the NEB²⁰ algorithm, which works by interpolating an initial path between reactant and product and iteratively updating it to minimize energy by using information about the PES. It shares a common bottleneck with other transition search algorithms – the necessity to repeatedly evaluate energy and atomic forces of molecular configurations, which is extremely costly, especially if ab-initio or electron DFT calculations are used²¹.

Recent advances in ML have not alleviated the bottleneck as even modern Neural Network (NN) architectures have not proved proficient

potential approximators for this type of application. The fault lies primarily with available data in the literature rather than the models’ expressiveness²². Most quantum mechanical datasets are focused on molecular configurations in or near equilibrium^{23,24,25,26}. Without configurations on and around reaction pathways in the training data, ML models cannot learn the interatomic interactions that occur during chemical reactions and cannot reliably be applied for transition-state search.

We compare ML models against DFTB,²⁷ a fast approximation to DFT that is often used for fast screening of large quantities of configurations with an acceptable trade-off between accuracy and speed, and our models outperform DFTB with a factor five in accuracy and a factor 2.5 in CPU time.

In this work, we bridge generalization, speed, and accuracy for transition-state search by applying Polarizable Atom interaction Neural Network (PaiNN) models as surrogate potentials for DFT. We build on and showcase the utility of our previous paper²⁸ where we released Transition1x, a dataset constituted by DFT calculations for 10 million molecular configurations, all sampled around reaction pathways from 10.000 elementary reactions. It is clear from the results of this paper, that for precise modeling of transition-state regions, and, consequently, transition states and barrier energies, hitherto popular benchmark datasets have had insufficient relevant data. On the other hand, training ML potentials on the Transition1x dataset allows for accurate modeling of PESs in transition-state regions, underlining that relevant and available data in the literature is as important as the efficiency of available models.

Reliable and fast analysis of reaction kinetics through ML will bring the whole field of computational chemistry a considerable step closer to the ultimate goal, a virtual laboratory, hyper-accelerating the discovery of reaction mechanisms for synthesizing drugs and materials.

2 Methods

2.1 Nudged Elastic Band

NEB²⁰ is a method for finding MEP and transition-state given product and reactant of a chemical reaction. It does so by iteratively nudging an interpolated path between the reaction endpoints in the direction of the force perpendicular to the path. Once the perpendicular force converges to zero, NEB reports the maximal-energy configuration along the path as the transition-state. The path is represented by an array of molecular configurations called images, and there is no guarantee that, at convergence, the maximal energy image corresponds to the maximal energy along the path. The maximum might lie between two images. Climbing Image Nudged Elastic Band (CINEB)²⁹ addresses this problem by letting the transition-state candidate (the maximal energy image) further maximize its energy by following the gradient on the PES parallel to the current path between iterations. If the current path has not converged properly, the climbing image can pull the predicted MEP off the true MEP and therefore, the path is first relaxed with regular NEB before turning on CINEB. The MEP is considered converged once the maximal perpendicular force on the path is below a threshold of 0.05 eV\AA^{-1} . The spring constant between images on the path is set to 0.1 eV\AA^{-2} , and ten images are used to represent the path.

2.2 Initial Path Generation

The endpoints of the reaction have to be minimized in their respective minima before running NEB – otherwise the energetic difference between reactant and transition-state cannot be evaluated properly. A configuration is considered relaxed if the norm of the forces acting on it is below 0.01 eV\AA^{-1} . Once the endpoints have been minimized, the initial guess for the MEP is found by running NEB with the Image Dependent Pair Potential (IDPP)³⁰ on a linearly interpolated path between reactant and product. IDPP is an inexpensive potential

specifically designed to generate physically realistic MEP guesses for NEB at an extremely low computational cost.

2.3 Optimizers

Reactants and products are relaxed using the BFGS³¹ optimizer with $\alpha = 70$ and a maximal step size of 0.03 \AA in configurational space. The MEP is found with an optimizer³² designed to reduce the computational cost of transition-state search algorithms by applying an adaptive time step selection algorithm with $\alpha = 0.01$ and $\text{rtol} = 0.1$, and a preconditioning scheme to the PES given an estimate of its curvature.

3 Data

We train all models on ANI1x²⁴, QM9x³³, Transition1x²⁸. All datasets are calculated with the 6-31G(d)³⁴ basis set and ω B97x³⁵ functional which has an accuracy comparable to the gold standard but expensive high-level CCSD(T)^{36,37} calculations. Given the compatibility of the datasets, it is possible to train on either dataset alone or combinations of them to leverage all of their strengths.

3.1 ANI1x

ANI1x³⁸ aims to provide varied data of off-equilibrium molecular configurations by perturbing equilibrium configurations with pseudo molecular dynamics. The data is collected through an active learning technique called Query by Committee; an automated data diversification process that trains an ensemble (committee) of models on a dataset and accepts or rejects new proposed data based on the disagreement of models in the committee. The assumption is that if the committee disagrees the data is sufficiently different from what has already been learned, and the proposed data should be included in the analysis. The procedure for proposing data and evaluating it with the committee is cheap compared to the calculation of data using DFT. The dataset is consecutively expanded by alternating between train-

ing committees and adding new data points based on the committee uncertainty. In total, ANI1x contains force and energy calculations for approximately 5 million configurations.

3.2 Transition1x

We have recently published Transition1x²⁸, a dataset providing a collection of molecular configurations on and along reaction paths for approximately 10,000 reactions. The reactions consist of up to 7 heavy atoms, including C, N, and O. Transition events are rare, and it is not possible to collect sufficient data in relevant regions by simple molecular dynamics if the intention is to train NNs models to understand chemical reactions. Transition1x addresses this problem by sampling molecular configurations around reaction pathways proposed by NEB, using DFT as potential. The procedure resulted in approximately 10 million DFT calculations that were collected and saved during the process and constitute the dataset. Transition1x is available through the repository <https://gitlab.com/matschreiner/Transition1x> which includes data loaders and scripts for downloading the dataset and generating ASE-database files.

3.3 QM9 and QM9x

QM9³³ is a dataset of 135k small organic molecules with various chemical properties that has served as the benchmark for many existing ML methods for quantum chemistry. All molecules in QM9 are in equilibrium. We have recalculated QM9 with the 6-31G(d) basis set and ω B97x functional to make it compatible with Transition1x and ANI1x, and we refer to the recalculated dataset as QM9x. Molecular configurations recalculated in the new potential are not necessarily in equilibrium as the potential shifts when changing functional and basis sets. QM9x is available through the repository <https://gitlab.com/matschreiner/QM9x> which includes data loaders and scripts for downloading the dataset and generating ASE-database files.

3.4 Models and Training

Message Passing Neural Networks (MPNNs)³⁹ are a class of GNNs^{1,2} that build their internal graph representation by running a series of message passing steps. A single message passing step consists of two distinct operations: i) *Message Dispatching*, each node computes a message given its state (and possibly information about the edge connecting to – and the state of the receiving node) and sends it to its neighbors. ii) *State Update*, incoming messages are collected with an aggregation function, and are used to simultaneously update the internal representation of all nodes. After the message-passing phase, a readout function extracts the inner representation of the nodes and computes a final feature vector of the graph for downstream tasks. In the case of molecules, interesting properties are energy and forces where conservative force fields can be computed via the back-propagation algorithm as the negative gradient of the energy wrt. coordinates of the atoms.

The PaiNN model⁴⁰ was used for all experiments – it is a GNN architecture that implements rotationally equivariant representations for prediction of tensorial properties of graph structures. We refer to the literature for further details⁴⁰. A cut-off radius of 5 Å was used to generate the initial molecular graph. All models have three message passing steps and 256 units in each hidden layer, and are trained using the ADAM⁴¹ optimizer with learning rate 10^{-3} on training examples from QM9x, ANI1x, and Transition1x. A batchsize of 75 was used for all datasets and a maximum of 10^6 training steps was allowed - however, models training on ANI1x and Transition1x reached maximal scores on validation data after around $6 \cdot 10^5$ steps. Transition1x was stratified by reactions without attention to reaction-type. 500 reactions were set aside for testing such that no data from around any test reaction was seen during training. 90% of the remaining data were used for training and the last 10% were used for validation and early stopping. ANI1x was stratified by chemical formula such

that test, validation and training sets consist of chemical formulas unique to that set. QM9x was split randomly. In the case of QM9x and ANI1x, 80% of the data was used for training, 10% for testing, and 10% was used for validation and early stopping. In QM9x all configurations are unique as they are in distinct equilibria and can therefore be split randomly. No attention was paid to the molecular scaffold. For ANI1x, it is necessary to split on chemical formula to ensure that configurations across splits are significantly different. Each chemical formula contains similar configurations, since data is generated by randomly perturbing identical initial configurations. In Transition1x the reactions follow unique paths in chemical space, and thus configurations between reactions are different. The Transition1x dataset forms a reaction network where the product from one reaction is the reactant for the next. Therefore, it is nontrivial to split it to get no shared reactants/products across train validation and test sets. We believe that our splitting is still useful because it achieves unique reaction paths and transition states between datasets.

4 Results

Table 1 shows the overall findings of the paper. Each row displays the performance of a surrogate potential, where datasets in the leftmost column indicate PaiNN models trained on the given dataset. The barrier error is the difference in barrier heights found when applying DFT as potential for NEB versus when applying the respective potential. As different initializations of parameters in equivalent architectures result in variations in the trained models, five models were trained on each dataset without changing training, testing and validation splits. These models were used as potentials for NEB, the table displays the mean and standard deviation of MAEs and RMSEs of each model.

The best models are trained on Transition1x, with the lowest MAE and RMSE and the high-

est convergence ratio. The QM9x models have only seen data very close to equilibrium and have not learned the structure of the PES between equilibria which makes it unable to converge in most cases. In general DFT performs the best in terms of convergence rate and average iterations run, but it comes at a steep price, running almost a factor 1500 times slower than the ML potentials. DFTB is the go-to fast potential, but the models trained on Transition1x are roughly 2.5 times faster and five times as accurate.

Figure 1, on the frontpage, displays MEPs calculated with NEB using DFT and PaiNN trained on Transition1x side by side. Each MEP is projected onto a plane in configurational space spanned by the reaction’s transition-state, product, and reactant. The x and y axes are basis vectors describing the plane in units of Å, and the z-axis and color-coding show the atomization energy of configurations in the plane in eV. Not only does PaiNN trained on the Transition1x accurately calculate the barrier energy for the reaction, but it also correctly identifies the plane spanned by the configurations defining the reaction, and calculates an almost identical PES in the vicinity of the MEP. Each MEP is projected from a high dimensional space onto the plane, and therefore, only the atomization energy of equilibria and transition-states are shown correctly in the plot. At these points, the MEP intersects with the plane. The intermediate points have energies slightly shifted up the sides of the energy valley. The MEP does not necessarily lie in the plane, and since the MEP represents the energy valley, projecting it onto the plane, will increase the energy. The \times symbols on the surfaces are projections of images predicted by NEB and the dashed lines connecting them are cubic spline interpolations. The importance of accurate predictions in the vicinity of the MEP is clear, as these calculations will guide the search for the transition-state. The Transition1x model predicts smooth and well-behaved PESs resembling DFT.

Figure 2 and 3 tell similar stories. Figure 2 is a histogram of barrier errors where the er-

	Barrier [eV]		NEB Convergence		
	MAE	RMSE	Rate	Avg. CPU Time	Avg. Iterations
ANI1x	0.43(1)	0.56(3)	71.9%	36s	130.91
T1x	0.13(3)	0.24(1)	80.5%	28s	111.97
QM9x	3.4(1)	3.6(1)	23.4%	26s	110.34
DFTB	0.66	0.79	72.0%	81s	115.65
DFT	-	-	84.1%	12h14m43s	100.74

Table 1: Performance of various potentials used for Nudged Elastic Band (NEB) when compared to Density Functional Theory (DFT). ANI1x, Transition1x and QM9x indicate PaiNN models trained on the respective dataset. The Barrier column displays the Mean Average Error (MAE) and Root Mean Squared Error (RMSE) of barrier predictions, where the individual error is the difference between the barrier as predicted when using DFT as potential vs. using the surrogate potential. The convergence rate is the percentage of reactions that converged. Average CPU time is CPU time spent per reaction. Average iterations is the average number of Minimal Energy Path (MEP) updates before convergence.

	MAE [eV]	RMSE [eV]	Systematic Error [eV]
ANI1x	0.40	0.56	0.16
DFTB	0.47	0.57	-0.55
Transition1x	0.17	0.30	-0.07

Table 2: MAE and Root Mean Squared Error (RMSE) of barrier errors found by PaiNN trained on Transition1x and ANI1x and DFTB, after correcting for systematic error.

ror is the difference between activation energy found using the surrogate potential and DFT. The Transition1x model is precise and accurate, with a sharp peak around zero, whereas DFTB and ANI1x have wider spreads with means below and above zero, respectively. The QM9x model is plotted on the histogram, but due to high errors and low convergence, only a few calculated barriers fall within an error of ± 1.5 eV, as shown in the figure. See appendix for an equivalent figure without truncated x-axis.

Figure 3 compares activation energies found with DFT on the x-axis with those found using various surrogate potentials on the y-axis. Each marker represents a single reaction. Predictions from the model trained on Transition1x follow the $x = y$ line with a MAE of only 0.13 eV. The QM9x model does not have a proper representation of the transition-state regions as it has not seen that type of data during training. Often, the QM9x model does not recognize nearby initial equilibria as minima on the PES, and even before optimizing the MEP, the reaction endpoints have dropped further

on the PES to qualitatively different endpoints which results in the model calculating the MEP for a completely different reaction. The algorithm is not set up to detect this, and as long as the reaction converges, it is included in the analysis. Even when the QM9x model relaxes the endpoints of the reaction correctly, it either finds low energy shortcuts in the faulty potential or does not converge, and as a result the converged reactions are often only the energy difference between reactant and product. The QM9x dataset was not designed with any type of molecular dynamics or reaction kinetics in mind, and comparing it to ANI1x and Transition1x for reaction path search is perhaps inappropriate. However, given the ubiquity of QM9 in the literature, it is an important point to convey, that new datasets are required for solving higher order problems in computational chemistry. The Transition1x and ANI1x models drop in performance above 5 eV. Data becomes scarcer at higher energies and consequently, models are less accurate in high energy regions. DFTB and the ANI1x models

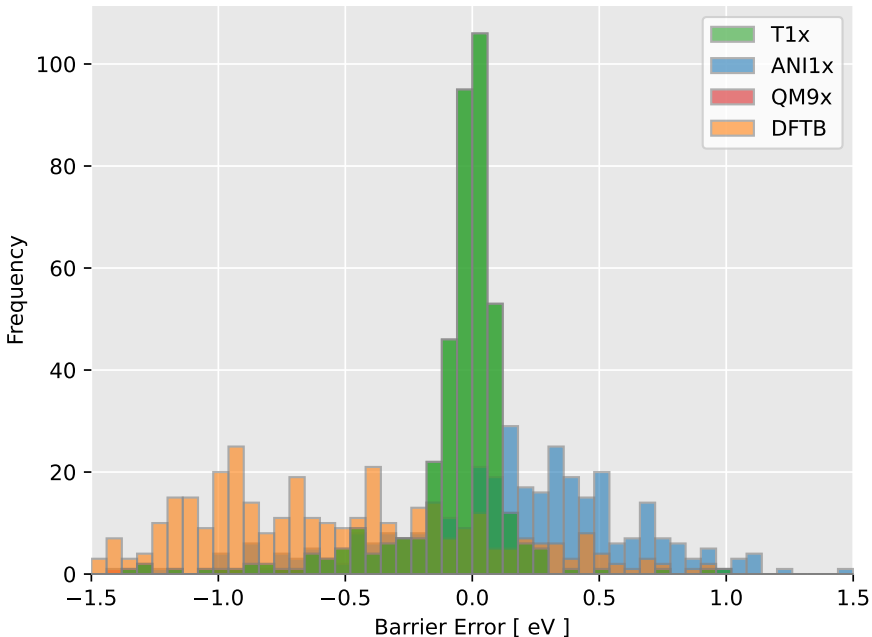


Figure 2: Histogram of barrier errors. The x-axis shows errors between reaction barriers calculated using Density Functional Theory (DFT) and surrogate potentials for Nudged Elastic Band (NEB). The x-axis has been truncated at ± 1.5 eV error (see appendix for the full plot). The y-axis shows the frequency of each bin. Green, red and blue display results from PaiNN models trained on Transition1x, QM9x and ANI1x, respectively. Yellow displays results from Density Functional based Tight Binding (DFTB). The QM9x model has such a low convergence frequency, and general barrier error, that the model does not show in the plot.

have systematic errors in their predictions. The ANI1x models are biased towards high energies in the transition regions as they have not seen the low energy valleys connecting equilibria. The DFTB potential systematically predicts energies too low. In Table 2 the systematic errors are corrected based on the training data. This leads to a lower test error for the ANI1x and DFTB, but a higher test error for Transition1x underlining that Transition1x models are already very accurate.

5 Discussion

To train models that can properly step in as surrogate potentials for DFT when running NEB, it is necessary to have datasets with appropriate data in and around transition-state regions.

Finding reaction barriers with ML models and NEB is a non-trivial test. ML models, and especially NNs, are known to perform poorly for out of distribution tasks^{42,43}. Table 3 illustrates this clearly with results for training and testing ML models on various datasets.

Finding reaction barriers with NEB is a much more demanding test of the models’ capabilities. When running NEB, the PES is swept by the path connecting endpoints, and data encountered in the process can diverge wildly from any data seen during testing and training. The model can get caught in even a small region of high error, or it can be thrown off the correct MEP and make it unable to converge altogether, so the model must be accurate across the entire PES.

The reaction paths are represented by ten

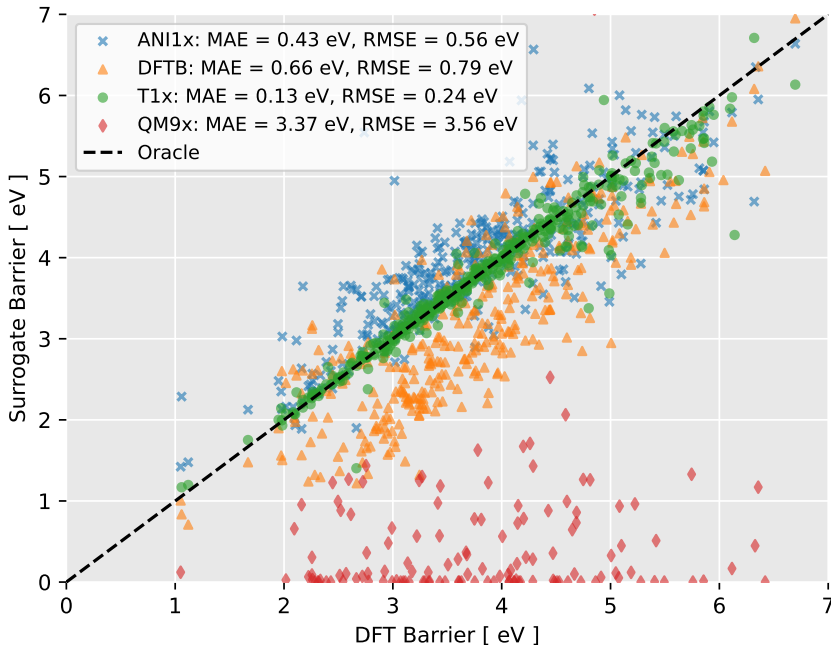


Figure 3: Comparison of reaction barriers found with Nudged Elastic Band (NEB) using Density Functional Theory (DFT) as potential on the x-axis vs. various surrogate potentials on the y-axis. Green, red and blue markers are PaiNN models trained on The Transition1x, QM9x, and ANI1x datasets respectively. Yellow is Density Functional based Tight Binding (DFTB). Points on the dashed line have been calculated perfectly.

images in all reactions. A core strength of NNs is their ability to utilize GPUs to evaluate multiple data points at once, and in principle, NEB can be run with hundreds of images instead of tens at little to no additional cost when using NNs as potentials. We ran experiments with high density paths with the rest of the setup fixed but saw no improvement in neither accuracy nor convergence speed. The preconditioning scheme of the NEB optimizer relies on a sparsely populated path. But this approach could possibly produce robust results by applying other optimizers.

A clear application of this work is as a screening procedure for complex reaction networks. Cheap methods, such as permuting bond order matrices, can be used to automatically generate nodes for entire reaction networks. The individual reactions can be screened fast using the method before recalculating entire reaction net-

works with expensive methods. Usually this is done with DFTB²⁷ but running NEB with NNs is faster and more accurate.

6 Conclusion

We have trained state-of-the-art GNN potentials on various datasets and used them as surrogate potentials for DFT when running NEB for transition-state search. A MAE of 0.13 eV and RMSE of 0.24 eV is achieved with the best model, compared against running the same set up with DFT. The models converge 80.5% of the time on unseen reactions. We show that expressive models alone are, by no means, sufficient for solving complex tasks in quantum chemistry moving forward, but just as much care has to be put into designing and generating datasets. We tested 3 different datasets:

ANI1x, QM9x and Transition1x and only models trained on the latter could reliably solve the transition search task.

Our results show that the future development of the field of ML for quantum chemistry stands on two legs – the completeness of the available data, and the expressiveness of the available models. Transition1x is a relatively simple dataset that deals with four types of atoms. To apply the results of this paper to general chemistry, larger datasets with more atom types should be produced. Our results indicate that the machine learning approach scales: With the right amount of the right data, accuracies at a sufficient level can be achieved.

Acknowledgements

The authors acknowledge support from the Novo Nordisk Foundation (SURE, NNF19OC0057822) and the European Union’s Horizon 2020 research and innovation program under Grant Agreement No. 957189 (BIG-MAP) and No. 957213 (BATTERY2030PLUS).

Ole Winther also receives support from Novo Nordisk Foundation through the Center for Basic Machine Learning Research in Life Science (NNF20OC0062606) and the Pioneer Centre for AI, DNRF grant number P1.

7 Code Availability

Code for training PaiNN models and running NEB is available through the repository <https://gitlab.com/matschreiner/neuralneb>.

References

- [1] Davide Bacciu, Federico Errica, Alessio Micheli, and Marco Podda. A gentle introduction to deep learning for graphs. *Neural Networks*, 129:203–221, 12 2019. doi: 10.1016/j.neunet.2020.06.006. URL <http://arxiv.org/abs/1912.12693><http://dx.doi.org/10.1016/j.neunet.2020.06.006>.
- [2] Jie Zhou, Ganqu Cui, Shengding Hu, Zhengyan Zhang, Cheng Yang, Zhiyuan Liu, Lifeng Wang, Changcheng Li, and Maosong Sun. Graph neural networks: A review of methods and applications. 2021. doi: 10.1016/j.aiopen.2021.01.001. URL <https://doi.org/10.1016/j.aiopen.2021.01.001>.
- [3] Felix A. Faber, Luke Hutchison, Bing Huang, Justin Gilmer, Samuel S. Schoenholz, George E. Dahl, Oriol Vinyals, Steven Kearnes, Patrick F. Riley, and O. Anatole Von Lilienfeld. Prediction errors of molecular machine learning models lower than hybrid dft error. *Journal of Chemical Theory and Computation*, 13:5255–5264, 11 2017. ISSN 15499626. doi: 10.1021/ACS.JCTC.7B00577/SUPPL_FILE/CT7B00577_SI_001.PDF. URL <https://pubs.acs.org/doi/abs/10.1021/acs.jctc.7b00577>.
- [4] Julia Westermayr, Michael Gastegger, Kristof T. Schütt, and Reinhard J. Maurer. Perspective on integrating machine learning into computational chemistry and materials science. *The Journal of Chemical Physics*, 154:230903, 6 2021. ISSN 0021-9606. doi: 10.1063/5.0047760. URL <https://aip.scitation.org/doi/abs/10.1063/5.0047760>.
- [5] Stuart I Campbell, Daniel B Allan, and Andi M Barbour. Machine learning for the solution of the schrödinger equation. *Machine Learning: Science and Technology*, 1:013002, 4 2020. ISSN 2632-2153. doi: 10.1088/2632-2153/AB7D30. URL <https://iopscience.iop.org/article/10.1088/2632-2153/ab7d30><https://iopscience.iop.org/article/10.1088/2632-2153/ab7d30/meta>.
- [6] Jörg Behler and Michele Parrinello. Generalized neural-network representation of high-dimensional potential-energy surfaces. *Physical review letters*, 98(14):146401, 2007.
- [7] Julia Westermayr and Philipp Marquetand. Machine learning for electronically excited states of molecules. *Chemical Reviews*, 121:9873–9926, 8 2021. ISSN 15206890. doi: 10.1021/ACS.CHEMREV.0C00749/ASSET/IMAGES/LARGE/CR0C00749_0011.JPEG. URL <https://pubs.acs.org/doi/full/10.1021/acs.chemrev.0c00749>.
- [8] Jean Louis Reymond. The chemical space project. *Accounts of Chemical Research*, 48:722–730, 3 2015. ISSN 15204898. doi: 10.1021/AR500432K/ASSET/IMAGES/LARGE/AR-2014-00432K_0003.JPEG. URL <https://pubs.acs.org/doi/full/10.1021/ar500432k>.
- [9] Jörg Behler and Michele Parrinello. Generalized neural-network representation of high-dimensional potential-energy surfaces. *Physical Review Letters*, 98:146401, 4 2007. ISSN 00319007. doi: 10.1103/PHYSREVLETT.98.146401/FIGURES/4/MEDIUM. URL <https://journals.aps.org/prl/abstract/10.1103/PhysRevLett.98.146401>.
- [10] Jörg Behler. Constructing high-dimensional neural network potentials: A tutorial review. *International Journal of Quantum Chemistry*, 115:1032–1050, 8 2015. ISSN 1097-461X. doi: 10.1002/QUA.24890. URL <https://onlinelibrary.wiley.com/doi/full/10.1002/QUA.24890>.

- 1002/qua.24890<https://onlinelibrary.wiley.com/doi/abs/10.1002/qua.24890><https://onlinelibrary.wiley.com/doi/10.1002/qua.24890>.
- [11] Felix A. Faber, Luke Hutchison, Bing Huang, Justin Gilmer, Samuel S. Schoenholz, George E. Dahl, Oriol Vinyals, Steven Kearnes, Patrick F. Riley, and O. Anatole Von Lilienfeld. Prediction errors of molecular machine learning models lower than hybrid dft error. *Journal of Chemical Theory and Computation*, 13:5255–5264, 11 2017. ISSN 15499626. doi: 10.1021/ACS.JCTC.7B00577/SUPPL_FILE/CT7B00577_SI_001.PDF. URL <https://pubs.acs.org/doi/abs/10.1021/acs.jctc.7b00577>.
- [12] Justin Gilmer, Samuel S Schoenholz, Patrick F Riley, Oriol Vinyals, and George E Dahl. Neural message passing for quantum chemistry. 2017.
- [13] Sami Kaappa, Casper Larsen, and Karsten Wedel Jacobsen. Atomic structure optimization with machine-learning enabled interpolation between chemical elements. *Physical Review Letters*, 127, 7 2021. doi: 10.1103/PhysRevLett.127.166001. URL <http://arxiv.org/abs/2107.01055><http://dx.doi.org/10.1103/PhysRevLett.127.166001>.
- [14] Jiaqi Wang, Seungha Shin, and Sangkeun Lee. Interatomic potential model development: Finite-temperature dynamics machine learning. *Advanced Theory and Simulations*, 3:1900210, 2 2020. ISSN 2513-0390. doi: 10.1002/ADTS.201900210. URL <https://onlinelibrary.wiley.com/doi/full/10.1002/adts.201900210><https://onlinelibrary.wiley.com/doi/abs/10.1002/adts.201900210><https://onlinelibrary.wiley.com/doi/10.1002/adts.201900210>.
- [15] M Malshe, LM Raff, MG Rockley, M Hagan, Paras M Agrawal, and R Komanduri. Theoretical investigation of the dissociation dynamics of vibrationally excited vinyl bromide on an ab initio potential-energy surface obtained using modified novelty sampling and feedforward neural networks. ii. numerical application of the method. *The Journal of chemical physics*, 127(13):134105, 2007.
- [16] Xiaoxiao Lu, Qingyong Meng, Xingan Wang, Bina Fu, and Dong H Zhang. Rate coefficients of the $\text{h} + \text{h}_2\text{O}_2 \rightarrow \text{h}_2 + \text{HO}_2$ reaction on an accurate fundamental invariant-neural network potential energy surface. *The Journal of chemical physics*, 149(17):174303, 2018.
- [17] Tom A Young, Tristan Johnston-Wood, Volker L Deringer, and Fernanda Duarte. A transferable active-learning strategy for reactive molecular force fields. *Chemical science*, 12(32):10944–10955, 2021.
- [18] Sergei Manzhos and Tucker Carrington Jr. Neural network potential energy surfaces for small molecules and reactions. *Chemical Reviews*, 121(16):10187–10217, 2020.
- [19] Olli Pekka Koistinen, Freyja B. Dagbjartsdóttir, Vilhjálmur Ásgeirsson, Aki Vehtari, and Hannes Jónsson. Nudged elastic band calculations accelerated with gaussian process regression. *Journal of Chemical Physics*, 147, 2017. ISSN 00219606. doi: 10.1063/1.4986787.
- [20] Daniel Sheppard, Rye Terrell, and Graeme Henkelman. Optimization methods for finding minimum energy paths. *The Journal of Chemical Physics*, 128:134106, 4 2008. ISSN 0021-9606. doi: 10.1063/1.2841941. URL <https://aip.scitation.org/doi/abs/10.1063/1.2841941>.
- [21] Stefan Heinen, Max Schwilk, Guido Falk von Rudorff, and O Anatole von Lilienfeld. Machine learning the computational cost of quantum chemistry. *Machine Learning: Science and Technology*, 1(2):025002, 2020.

- [22] O. Anatole von Lilienfeld, Klaus Robert Müller, and Alexandre Tkatchenko. Exploring chemical compound space with quantum-based machine learning. *Nature Reviews Chemistry* 2020 4:7, 4:347–358, 6 2020. ISSN 2397-3358. doi: 10.1038/s41570-020-0189-9. URL <https://www.nature.com/articles/s41570-020-0189-9>.
- [23] Justin S. Smith, Olexandr Isayev, and Adrian E. Roitberg. Ani-1, a data set of 20 million calculated off-equilibrium conformations for organic molecules. *Scientific Data* 2017 4:1, 4: 1–8, 12 2017. ISSN 2052-4463. doi: 10.1038/sdata.2017.193. URL <https://www.nature.com/articles/sdata2017193>.
- [24] Justin S. Smith, Roman Zubatyuk, Benjamin Nebgen, Nicholas Lubbers, Kipton Barros, Adrian E. Roitberg, Olexandr Isayev, and Sergei Tretiak. The ani-1ccx and ani-1x data sets, coupled-cluster and density functional theory properties for molecules. *Scientific Data* 2020 7:1, 7:1–10, 5 2020. ISSN 2052-4463. doi: 10.1038/s41597-020-0473-z. URL <https://www.nature.com/articles/s41597-020-0473-z>.
- [25] Tobias Fink and Jean Louis Raymond. Virtual exploration of the chemical universe up to 11 atoms of c, n, o, f: Assembly of 26.4 million structures (110.9 million stereoisomers) and analysis for new ring systems, stereochemistry, physicochemical properties, compound classes, and drug discovery. *Journal of Chemical Information and Modeling*, 47:342–353, 2007. ISSN 1549960X. doi: 10.1021/CI600423U.
- [26] Tobias Fink, Heinz Bruggesser, and Jean Louis Reymond. Virtual exploration of the small-molecule chemical universe below 160 daltons. *Angewandte Chemie - International Edition*, 44: 1504–1508, 2 2005. ISSN 14337851. doi: 10.1002/ANIE.200462457.
- [27] Gotthard Seifert and Jan Ole Joswig. Density-functional tight binding—an approximate density-functional theory method. *Wiley Interdisciplinary Reviews: Computational Molecular Science*, 2:456–465, 5 2012. ISSN 1759-0884. doi: 10.1002/WCMS.1094. URL <https://onlinelibrary.wiley.com/doi/full/10.1002/wcms.1094><https://onlinelibrary.wiley.com/doi/abs/10.1002/wcms.1094><https://wires.onlinelibrary.wiley.com/doi/10.1002/wcms.1094>.
- [28] Mathias Schreiner, Arghya Bhowmik, Tejs Vegge, Jonas Busk, and Ole Winther. Transition1x. 6 2022. doi: 10.6084/m9.figshare.19614657.v4. URL <https://figshare.com/articles/dataset/Transition1x/19614657>.
- [29] Graeme Henkelman, Blas P. Uberuaga, and Hannes Jónsson. A climbing image nudged elastic band method for finding saddle points and minimum energy paths. *The Journal of Chemical Physics*, 113:9901, 11 2000. ISSN 0021-9606. doi: 10.1063/1.1329672. URL <https://aip.scitation.org/doi/abs/10.1063/1.1329672>.
- [30] Søren Smidstrup, Andreas Pedersen, Kurt Stokbro, and Hannes Jónsson. Improved initial guess for minimum energy path calculations. *The Journal of Chemical Physics*, 140:214106, 6 2014. ISSN 0021-9606. doi: 10.1063/1.4878664. URL <https://aip.scitation.org/doi/abs/10.1063/1.4878664>.
- [31] C. G. Broyden. The convergence of a class of double-rank minimization algorithms 1. general considerations. *IMA Journal of Applied Mathematics*, 6:76–90, 3 1970. ISSN 0272-4960. doi: 10.1093/IMAMAT/6.1.76. URL <https://academic.oup.com/imamat/article/6/1/76/746016>.

- [32] Stela Makri, Christoph Ortner, and James R. Kermode. A preconditioning scheme for minimum energy path finding methods. *The Journal of Chemical Physics*, 150:094109, 3 2019. ISSN 0021-9606. doi: 10.1063/1.5064465. URL <https://aip.scitation.org/doi/abs/10.1063/1.5064465><http://creativecommons.org/licenses/by/4.0/>.
- [33] Raghunathan Ramakrishnan, Pavlo O. Dral, Matthias Rupp, and O. Anatole Von Lilienfeld. Quantum chemistry structures and properties of 134 kilo molecules. *Scientific Data* 2014 1:1, 1:1–7, 8 2014. ISSN 2052-4463. doi: 10.1038/sdata.2014.22. URL <https://www.nature.com/articles/sdata201422>.
- [34] R. Ditchfield, W. J. Hehre, and J. A. Pople. Self-consistent molecular-orbital methods. ix. an extended gaussian-type basis for molecular-orbital studies of organic molecules. *The Journal of Chemical Physics*, 54:724, 9 2003. ISSN 0021-9606. doi: 10.1063/1.1674902. URL <https://aip.scitation.org/doi/abs/10.1063/1.1674902>.
- [35] Jeng Da Chai and Martin Head-Gordon. Systematic optimization of long-range corrected hybrid density functionals. *The Journal of Chemical Physics*, 128:084106, 2 2008. ISSN 0021-9606. doi: 10.1063/1.2834918. URL <https://aip.scitation.org/doi/abs/10.1063/1.2834918>.
- [36] Kevin E. Riley, Michal Pitončák, Petr Jurecčka, and Pavel Hobza. Stabilization and structure calculations for noncovalent interactions in extended molecular systems based on wave function and density functional theories. *Chemical Reviews*, 110:5023–5063, 9 2010. ISSN 00092665. doi: 10.1021/CR1000173.
- [37] Kanchana S. Thanthiriwatte, Edward G. Hohenstein, Lori A. Burns, and C. David Sherrill. Assessment of the performance of dft and dft-d methods for describing distance dependence of hydrogen-bonded interactions. *Journal of Chemical Theory and Computation*, 7:88–96, 1 2011. ISSN 15499618. doi: 10.1021/CT100469B.
- [38] Justin S. Smith, Ben Nebgen, Nicholas Lubbers, Olexandr Isayev, and Adrian E. Roitberg. Less is more: Sampling chemical space with active learning. *The Journal of Chemical Physics*, 148:241733, 5 2018. ISSN 0021-9606. doi: 10.1063/1.5023802. URL <https://aip.scitation.org/doi/abs/10.1063/1.5023802>.
- [39] Justin Gilmer, Samuel S Schoenholz, Patrick F Riley, Oriol Vinyals, and George E Dahl. Neural message passing for quantum chemistry. 2017.
- [40] Kristof T Schütt, Schütt, Oliver T Unke, and Michael Gastegger. Equivariant message passing for the prediction of tensorial properties and molecular spectra. 2021.
- [41] Diederik P Kingma and Jimmy Lei Ba. Adam: A method for stochastic optimization.
- [42] Jens Henriksson, Christian Berger, Markus Borg, Lars Tornberg, Sankar Raman Sathyamoorthy, and Cristofer Englund. Performance analysis of out-of-distribution detection on various trained neural networks. 2021. URL <https://www.iso.org/deliverables-all.html>.
- [43] Lily H Zhang, Mark Goldstein, and Rajesh Ranganath. Understanding failures in out-of-distribution detection with deep generative models. 2021.

A PaiNN Performance On Test Data

Table displaying results of the models when training and testing on various datasets. In all test set-ups the models that perform best, are models that have been trained on training data from the corresponding dataset.

Trained on	Tested on	Energy [eV]		Forces [eV/Å]	
		RMSE	MAE	RMSE	MAE
ANI1x	ANI1x	0.04(1)	0.02(0)	0.04(0)	0.01(0)
Transition1x		0.35(2)	0.22(1)	0.34(2)	0.08(0)
QM9x		3.03(2)	2.32(1)	1.3(7)	0.56(2)
ANI1x	Transition1x	0.61(7)	0.28(2)	0.5(1)	0.10(5)
Transition1x		0.10(1)	0.05(0)	0.10(0)	0.04(1)
QMx		2.61(2)	1.42(1)	0.43(0)	0.19(0)
ANI1x	QM9x	0.13(0)	0.12(0)	0.05(0)	0.02(0)
Transition1x		0.12(0)	0.07(1)	0.07(0)	0.04(0)
QM9x		0.04(2)	0.02(1)	0.01(0)	0.01(0)

Table 3: Test results of PaiNN models trained on ANI1x, QM9x, Transition1x. We report RMSE and MAE on energy and forces. Force error is the Euclidian distance between the predicted and true force vector.

B Additional Figures

This section contains the unbounded version of Fig. 2 as well as additional plots of MEPs and PESs comparing PaiNN trained on Transition1x with DFT.

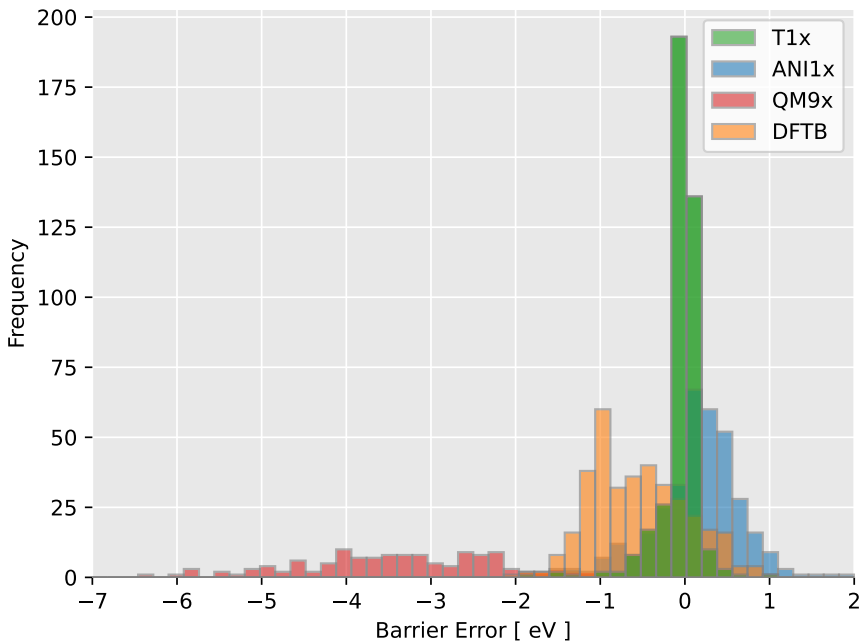


Figure 4: Histogram of barrier errors. The x-axis shows errors between reaction barriers calculated using Density Functional Theory (DFT) and surrogate potentials for Nudged Elastic Band (NEB). The y-axis shows the frequency of each bin. Green, red and blue display results from PaiNN models trained on Transition1x, QM9x and ANI1x, respectively. Yellow displays results from Density Functional based Tight Binding (DFTB). The QM9x model has such a low convergence frequency, and general barrier error, that the model does not show in the plot.

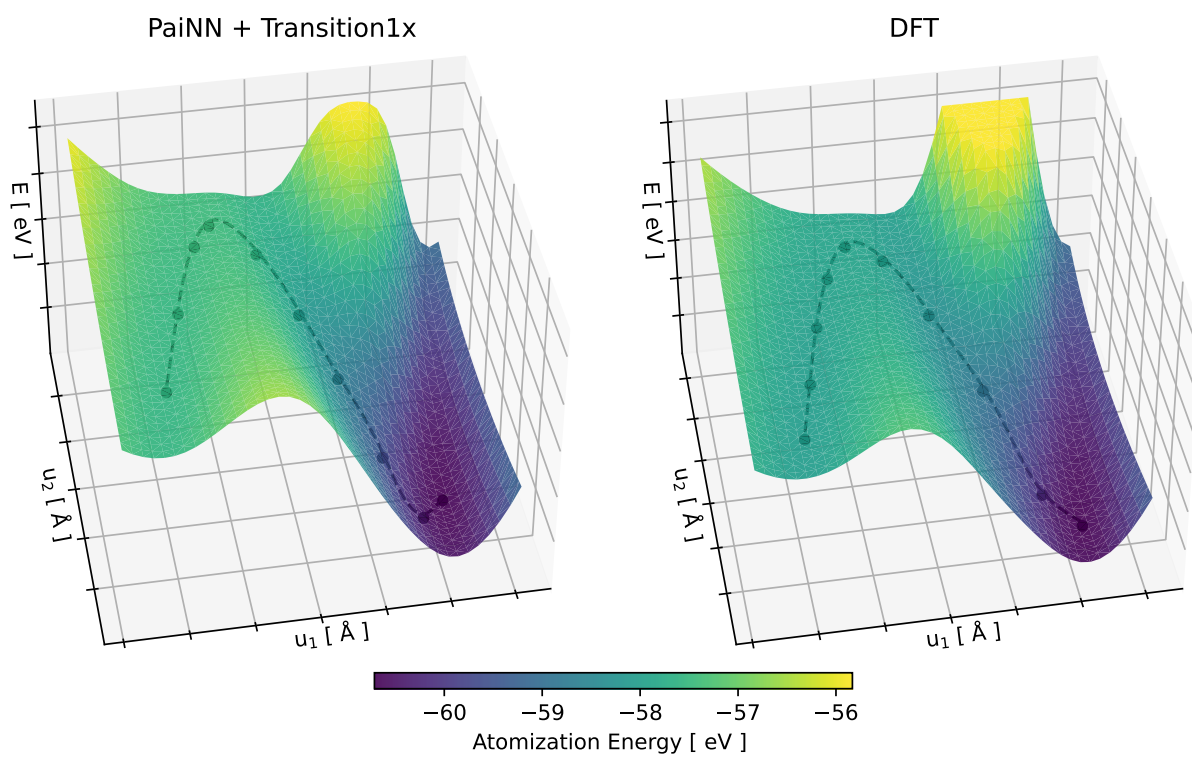


Figure 5: Reaction involving C5OH8. The reaction can be seen as a GIF by following [this link](#).

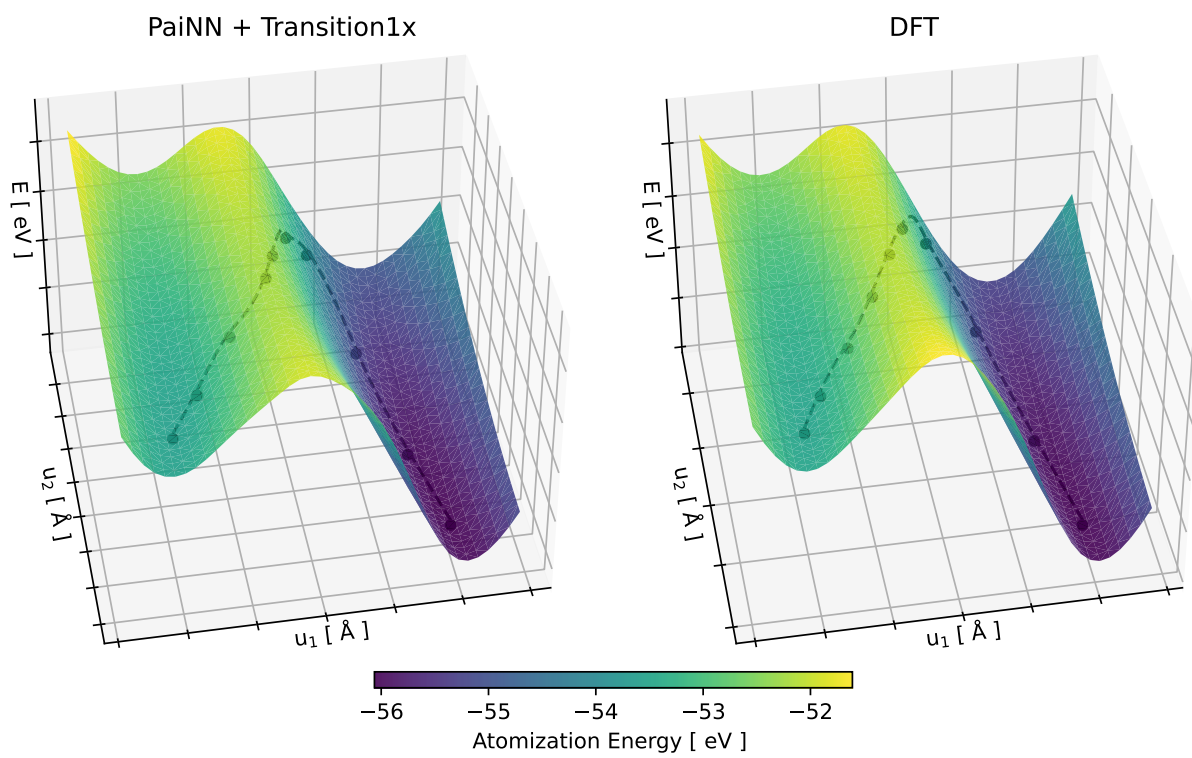


Figure 6: Reaction involving C3NCOH7. The reaction can be seen as a GIF by following [this link](#).

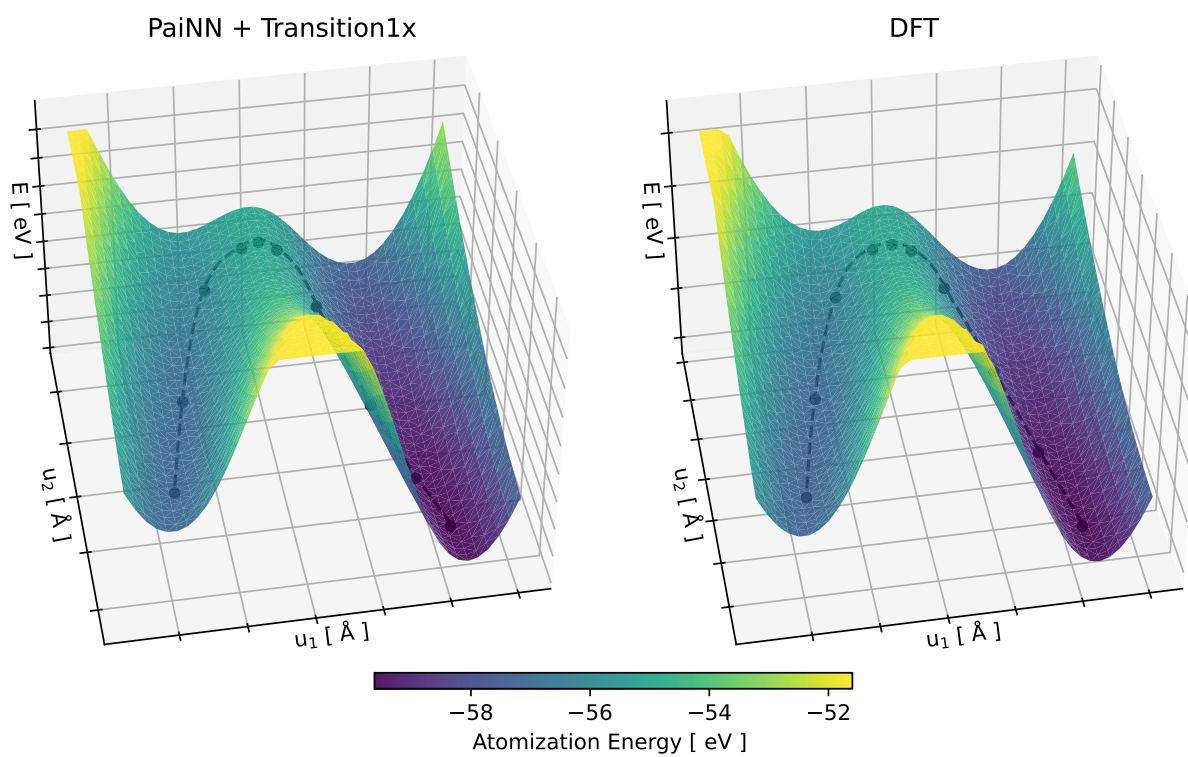


Figure 7: Reaction involving C3NCNH8. The reaction can be seen as a GIF by following [this link](#).

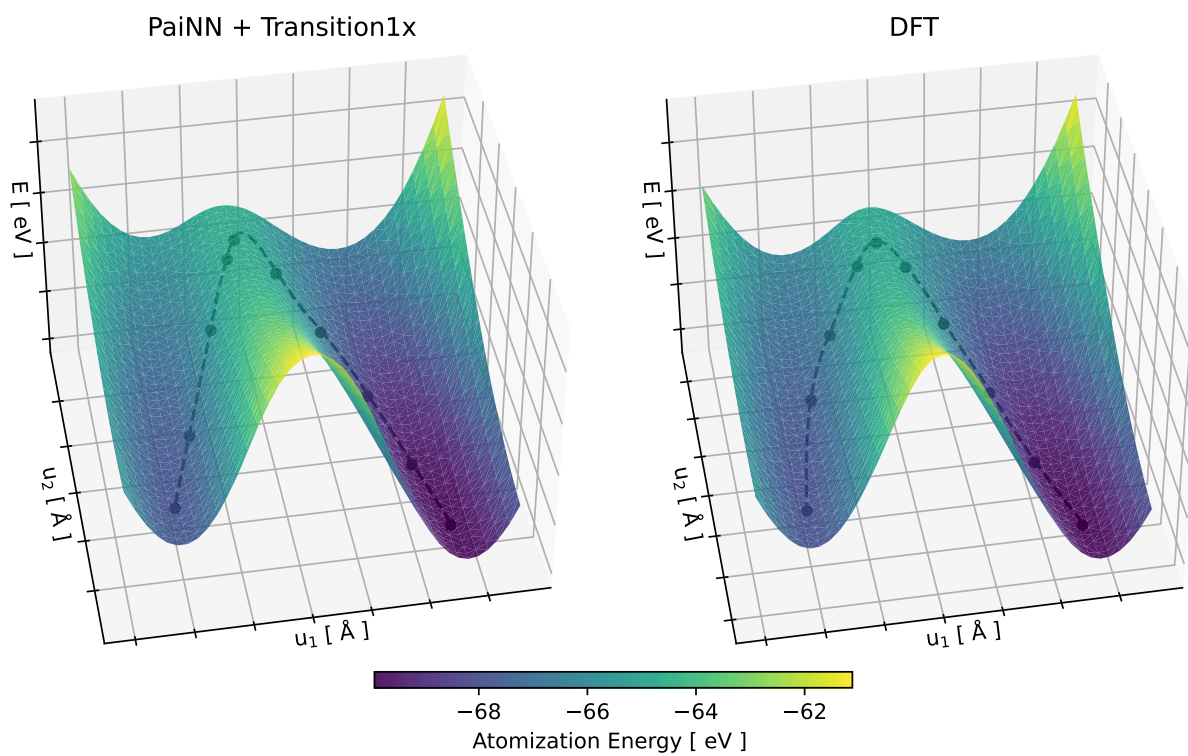


Figure 8: Reaction involving C3NC2OH9. The reaction can be seen as a GIF by following [this link](#).